Glucose-Responsive Fibrin Hydrogel-Based Multimodal Nucleic Acid Delivery System

Mangesh Morey, Aitor Larrañaga, Sunny Akogwu Abbah, Raghvendra Bohara, Amal Aljaabary, and Abhay Pandit*

Nucleic acid therapy has emerged as a potential alternative for promoting wound healing by gene expression modification. On the other hand, protecting the nucleic acid payload from degradation, efficient bioresponsive delivery and effective transfection into cells remain challenging. A glucose-responsive gene delivery system for treating diabetic wounds would be advantageous as it would be responsive to the underlying pathology giving a regulated payload delivery with fewer side effects. Herein a GOx-based glucose-responsive delivery system is designed based on fibrin-coated polymeric microcapsules (FCPMC) using the layer-by-layer (LbL) approach that simultaneously delivers two nucleic acids in diabetic wounds. The designed FCPMC displays an ability to effectively load many nucleic acids in polyplexes and release it over a prolonged period with no cytotoxic effects seen in in vitro studies. Furthermore, the developed system does not show any undesired effects in vivo. When applied to wounds in genetically diabetic db/db mice, the fabricated system on its own improves reepithelialization and angiogenesis while decreasing inflammation. Also, key proteins involved in the wound healing process, i.e., Actn2, MYBPC1, and desmin, are upregulated in the glucose-responsive fibrin hydrogel (GRFHG) treated group of animals. In conclusion, the fabricated hydrogel promotes wound healing. Furthermore, the system may be encapsulated with various therapeutic nucleic acids that aid wound healing.

1. Introduction

Nucleic acid therapy can modulate several lethal disease states,[1] including cancer, Alzheimer's disease, and atherosclerosis. The naked plasmid is the safest approach for gene delivery, but its use is limited because of its low transfection rate.[2] Various nucleic acid carriers, including viral and non-viral, have been studied.[3] Viral vectors provide a higher transfection rate but are limited in use because of inherent cytotoxicity issues.[4] Conversely, non-viral carriers are safe, but further improvement is needed in their transfection efficacy.[5] Different strategies have been used to enhance nucleic acid delivery through non-viral gene carriers, i.e., physical and chemical methods.[6] However, none of these methods provides sufficient therapeutic delivery.[2–6]

Depending on the intensity or concentration of stimulus, a responsive delivery system can provide pulsative release kinetics and facilitate a longer therapeutic delivery in the required space. A glucose-responsive nucleic acid delivery platform will be valid as the diabetic wound has the inherent glucose trigger. A topical nucleic acid delivery method is ideal for wound healing because it is minimally invasive and can treat a large surface area.[7–9] Many studies suggest an improvement of diabetic wounds by using nucleic acid therapy.[9–11] Lee et al. showed an accelerated reepithelialization, increased fibroblast proliferation, as well as organized and mature collagen fibers at the early stage of the healing process with the delivery of naked plasmid transforming growth factor-beta (TGF-beta) through a thermo-sensitive hydrogel made up of a triblock copolymer, and PEG (polyethylene glycol)-PLGA (poly (lactic-co-glycolic acid))-PEG.[11] The topical application of Rab18-eNOS genes enhanced wound closure by increasing functional angiogenesis and reducing inflammation in an alloxan-induced hyperglycemic preclinical ear ulcer model of compromised wound healing.[12]

Most of the delivery mentioned above methods lack effective control over drug delivery kinetics. Hence the attention has shifted toward responsive and disease-specific delivery systems as an effective system due to optimal payload delivery at the targeted site. We believe glucose-responsive nucleic acid therapy for treating hyperglycemic wounds will be the most appropriate and effective control release kinetics. Three main glucose-responsive delivery systems have been reported in the literature: boronate, concanavalin A, and glucose oxidase (GOx).[13] As boronate lack of specificity for glucose, and concanavalin A

M. Morey, A. Larrañaga, S. A. Abbah, R. Bohara, A. Aljaabary, A. Pandit
CÚRAM
SFI Research Centre for Medical Devices
University of Galway
Galway Ireland
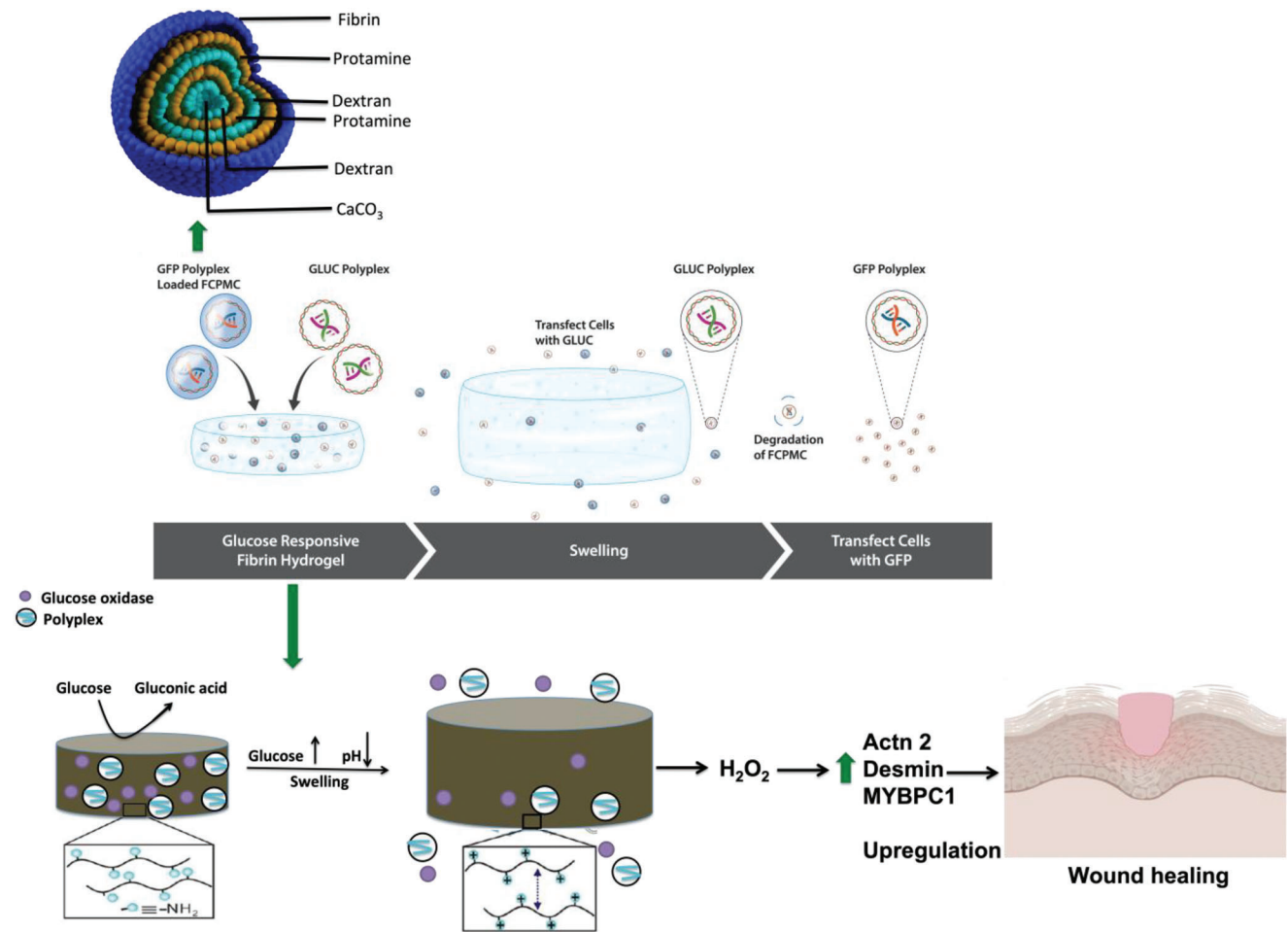E-mail: abhay.pandit@universityofgalway.ie

Figure 1. Overview of the developed glucose-responsive dual nucleic acid delivery system. The system was assembled with fabricated scaffolds, i.e., Fibrin-coated polymeric microcapsules (FCPMC) and glucose-responsive fibrin hydrogel (GRFHG) loaded with reporter plasmids, mainly GFP and Gaussia Luciferase (GLuc) polyplexes. In the presence of glucose, GRFHG swells by the action of glucose oxidase (GOx). The swelling facilitates the release of GFP and GLuc polyplexes, and the released polyplexes transfect the cells. Also, the minute quantity of H_2O_2 by-product generated during the reaction of GOx on glucose improves wound healing.

raises host immunological responses, GOx is considered the option with greater validity due to its added advantages like sensitivity,[13–15] making this system a potential candidate in wound healing. A minute quantity of hydrogen peroxide generated by the reaction of GOx with glucose is expected to have a huge health benefit in wound healing. However, the GOx-based systems are slow and unpredictable.[16]

Considering this herein, we have designed a GOx-based glucose-responsive delivery system that simultaneously delivers two nucleic acids in diabetic wounds (**Figure 1**). The system generates hydrogen peroxide as a lower-quality side product, essential for wound healing. We have used fibrin, a well-accepted biomaterial that is pH-sensitive (in acidic conditions such as in the presence of gluconic acid, amines present in the fibrin protonates and repel each other), resulting in swelling and subsequent payload release from the system (Figure 1). We have designed fibrin-coated polymeric microcapsules (FCPMC) by using the layer-by-layer (LbL) approach on the synthesized calcium carbonate ($CaCO_3$) template. The reporter gene green fluorescent protein (GFP) has been loaded within FCPMC. The GFP-loaded

FCPMC were encapsulated in the glucose-responsive fibrin hydrogel (GRFHG), which contains the second reporter gene, i.e., Gaussia Luciferase (GLuc). Finally, a genetically diabetic db/db mouse model obtained the developed system's glucose-responsive dual nucleic acid delivery. The system has been topically applied to the wound of genetically diabetic db/db mice. Additionally, we have evaluated the therapeutic effects of the developed system on angiogenesis and inflammation in a genetically diabetic db/db mouse model.

2. Materials

Protamine sulfate salt from Salmon, Ethylenediaminetetraacetic acid disodium salt (EDTA-Disodium salt dihydrate), Dextran sulfate salt from Leuconostoc spp., GOx, Fibrinogen, Thrombin, D-glucose, Sodium carbonate, Calcium chloride, Proteinase K, and Dimethyl sulfoxide (DMSO) from Sigma–Aldrich. alamarBlue™ assay kit from Life Technologies, Ireland, Live/Dead® staining kit from Life Technologies, Ireland, Dialysis membrane of pore size 4–6 kDa from Fisher, Mirus Label IT® Cy3™

2300161 (2 of 18)

labelling kit, Xfect™ Transfection reagent from Takara Bio, Tegaderm/Bioclusive Film from Medguard Healthcare Ltd, sodium pentobarbital. Anti-CD31 antibody: ab28364, Anti-CD68 antibody: ab28364, Alpha-actinin-2 (Actn2) antibody: Abcam-Ab9465, from Abcam, UK, Alexafluore 546 secondary antibodies Life Technologies, Ireland, Trypsin, Phosphate-Buffered Saline with Tween 20 (PBST), Urea from Fisher Scientific, Ireland, Desmin antibody (Santa Cruz Biotechnology sc-23879), myosin binding protein-C 1 (MYBPC1) antibody (Proteintech22900-1-AP). All other chemicals used were of analytical grade.

3. Methods

3.1. Synthesis of Calcium Carbonate Template

The $CaCO_3$ template was synthesized from Na_2CO_3 and $CaCl_2$ by the co-precipitation method. Briefly, 1 M solution of Na_2CO_3 was dropped into the stirring 1 M solution of $CaCl_2$ for 30 s to form the $CaCO_3$ spherical template. Immediately after $CaCO_3$ formation, this was allowed to settle for 1 min without disturbing it. The formed template was then washed twice with distilled water.

3.2. LbL Assembly

On the synthesized $CaCO_3$ template, different layers of natural polyelectrolytes were coated by electrostatic interaction. Polyelectrolytes like dextran, protamine, and fibrinogen were dissolved at a 1 mg mL^{-1} concentration in a 0.5 M NaCl solution. Dextran sulfate was the choice of polyelectrolytes for the first layer due to the negative charge. The organization of the different layers was as follows: dextran, protamine, dextran, protamine, and fibrinogen (Figure 1). Each layer was coated for 15 min. under stirring at 500 revolutions per minute (r/min), and the template was washed two times with 5 mM NaCl after each coating to remove any unbound polyelectrolytes. The zeta potential measurement ensured the coating of each layer by using a zeta sizer (Malvern, Nano-ZS90) at neutral pH in 0.05 mM NaCl.

Once the five layers had been coated on the surface, the template was sacrificed using an EDTA solution (1 M, pH 6.5-7.0). To remove the $CaCO_3$ core altogether, EDTA was applied four times. After that, the hollow polymeric microcapsules were crosslinked with 10 µL of human thrombin (100 units mL^{-1}) for 10 min under gentle stirring. Finally, the fabricated FCPMCs were washed with distilled water. The morphological characterization was done with SEM, transmission electron microscopy (TEM), and zeta size measurement. SEM analysis was used for surface morphological analysis of FCPMC. The sample was gold coated and visualized under vacuum using SEM (Hitachi S-4700 Scanning Electron Microscope). The FCPMC sample was prepared for TEM as follows: the FCPMCs were suspended in water. A drop was placed directly on a carbon-coated grid (Agar Scientific) and viewed under TEM (Hitachi H7500 transmission electron microscope). The mean size of FCPMCs was measured by laser light diffraction using a zeta sizer (Nano ZS, Malvern). The air-dried FCPMCs were suspended directly in water and vortexed gently. The particle size is expressed as mean diameter (± standard deviation). The complete removal of the $CaCO_3$ template

was ensured by EDX analysis. After gold coating, the sample was analyzed for different elements. The average charge on the surface of fabricated FCPMC was analyzed by zeta potential measurement using the zeta sizer (Malvern, Nano-ZS90).

3.3. Presence of Fibrin in FCPMC

The presence of fibrin in the FCPMC was determined using fluorescein isothiocyanate (FITC)-labelled fibrinogen. Fibrinogen (10 mg) dissolved in 500 µL of carbonate buffer (500 mM, pH 9.5). The FITC solution was prepared in DMSO at 1 mg mL^{-1}. The FITC solution was added to the fibrinogen solution at a 1:1 ratio and allowed to react for 30 min at room temperature under dark. After labelling, the unreacted FITC molecules were removed by dialysis in phosphate-buffered saline (PBS) overnight. A dialysis membrane of 4–6 kDa size was used for dialysis. The FITC-labelled fibrinogen solution was used to fabricate FCPMCs. The fluorescence was observed from FCPMC under a fluorescent microscope to confirm fibrin's presence.

3.4. Cytocompatibility

3.4.1. Alamarblue^{tm} cell Metabolic Activity Assay

A synthesized microcapsule's ability to preserve the metabolic activity of NHEK was quantified using the alamarBlue™ cell metabolic activity assay. Briefly, 5000 cells/well were seeded into the 96 well plates, and the cells were allowed to grow overnight. A different number of FCPMC was incubated with the cells for 24 and 48 h. After completing the incubation period, the supernatant of the FCPMC was removed with a pipette, and a 10% alamarBlue™ solution was added to each of the wells for 4 h. The cells without FCPMC were used as a control.

3.4.2. Live and Dead Assay

In an eight-chamber slide, 10 000 NHEK cells/chamber were seeded. Different doses of the FCPMC were added to each chamber for 48 h. Then FCPMCs were washed with PBS and incubated with 10 mM calcein-AM green (Life Technologies, Ireland) and 1 mM ethidium homodimer-1 (Life Technologies, Ireland) for 30 min. The sample images were taken with a fluorescence microscope (Olympus BX51, Ireland). The cells without FCPMC were used as a control.

3.4.3. Biodegradability of the FCPMC

90 mg of synthesized FCPMC was used in a biodegradability study. To the suspended FCPMC, 100 µL of 2 mg mL^{-1} proteinase K was added to water (final conc. 1 mg mL^{-1}). The FCPMC and proteinase K were incubated at 37 °C overnight. The degradation of FCPMCs was observed by SEM analysis.

3.5. Encapsulation of Nucleic Acid

To check the feasibility of FCPMC as a nucleic acid depot, GFP plasmid was encapsulated within FCPMC. First, the GFP plasmid was labelled with Cy3 labelling following the manufacturer's

**ADVANCED
SCIENCE NEWS**

www.advancedsciencenews.com

**ADVANCED
BIOLOGY**

www.advanced-bio.com

instructions. Mirus Label IT® Cy3™ labelling kit was used for the labelling. Briefly, this required warming the label IT reagent at room temperature followed by a quick spin. Then, 100 µL of reconstitution solution was added to the reagent and mixed well. An equal volume of 1 mg mL^{-1} GFP and label IT reagent was mixed well and incubated at 37 °C for 1 h. The labelled pDNA was purified by using G50 micro spin purification columns.

The column was placed in a sterile 1.5 mL microcentrifuge tube for support. Then the column was centrifuged for 1 min at 735 x g, and the buffer was discarded. The column was placed in a new 1.5 mL microcentrifuge tube. The column was centrifuged at 735 x g for 2 min 50 µL of the sample was slowly added to the resin's top without disturbing the resin bed. The purified sample was then collected in a microcentrifuge tube. After GFP labelling with Cy3, it was complexed with a nonviral transfection agent (Xfect™). 1:20 ratio of the plasmid: transfection agent was used. This labelled and complexed pDNA was encapsulated within the FCPMC. After loading, the FCPMC and Cy3 GFP were viewed under an inverted fluorescent microscope.

3.6. Release of Cy3 Labelled GFP Polyplex from FCPMC

2 µg of Cy3 labelled GFP polyplexes were encapsulated within FCPMC by diffusion. Encapsulated FCPMCs were dissolved in 500 µL of PBS solution. 50 µL supernatant solution was collected for the analysis at each time point, and the same amount of PBS was replaced. A standard curve was prepared using cy3 labelled GFP polyplex by measuring fluorescence intensity. The amount of polyplex present at each time point in the releasing medium was determined by the intensity measured in a spectrophotometer (Varioskan Flash, Thermo Fisher Scientific).

3.7. Transfection Studies

Parameters such as plasmid: polymer ratio dose optimization were optimized to achieve successful transfection. Two reporter genes, i.e., GFP, GLuc cells were investigated in two cell lines normal human keratinocytes (NHEK) cells and NIH3T3 for the transfection studies.

3.8. Plasmid: Polymer Ratio Optimization

First, the plasmid: polymer ratio was optimized for gLuc and GFP polymers. Agarose gel electrophoresis was used to check free and complexed plasmids. The optimized plasmid: polymer was used for all subsequent transfection experiments.

3.8.1. GLuc Plasmid

A range of different plasmids: polymer ratios, i.e., 1:0.7, 1:2, 1:3.5, 1:7, 1:20, has been used to obtain the optimal complexation concentration for transfection. An agarose gel electrophoresis was run to find the best concentration to complete the complexation. A transfection experiment was conducted using NIH3T3 cells to confirm the plasmid: polymer ratio. The widely used complexation reagent polyethyleneimine (PEI) was used as a positive control, while naked plasmid was used as a negative control. The cell

transfection was analyzed after 48 h by luciferase assays using a Biolux luciferase assay kit (Biolab).

3.8.2. GFP Plasmid

As with the gLuc plasmid above, similar experiments for GFP were conducted using agarose gel electrophoresis, and the transfection of GFP positive cells was assessed using an inverted fluorescence microscope.

3.8.3. Optimization of gLuc Polyplex Dose in Keratinocytes

Optimization of gLuc polyplex concentration for transfection in keratinocytes has been investigated. A series of experiments, i.e., transfection, cell metabolic activity and PicoGreen® assay, was conducted to determine the polyplex concentration for higher transfection of keratinocytes without affecting cellular activity. A few polyplex concentrations were used (Data not shown), but we choose 1 µg for subsequent transfection experiments because doses higher than this were toxic to the cells. For the transfection study, 50 000 keratinocytes cells/well were seeded in a 12-well plate. After overnight incubation, 1 µg polyplexes were added to the cells for 4 h. PEI was used as a positive control, and naked plasmid was used as a negative control. The polyplex solution was replaced by the regular growth medium and incubated for 48 h. The quantification of transfection was determined by luciferase assay as described earlier. Any undesired effect on the keratinocyte's metabolic activity was assessed using the alamarBlue™ assay following instructions given by the manufacturer. Then, the quantity of DNA was determined by PicoGreen® assay following the manufacturer's instructions.

3.8.4. Optimization of GFP Polyplex Dose in Keratinocytes

Similar experiments for GFP were conducted as those with gLuc. Briefly, in a 12 well plate, 50 000 cells/well were seeded and incubated overnight for an attachment. Then, (a) 1 µg polyplex dose was added to the cells and incubated for 4 h. After 4 h, the polyplex solution was replaced with the regular growth medium and incubated transfected cells for 48 h. The transfected cells were observed using an inverted fluorescence microscope. Any undesired effect on the metabolic activity of keratinocytes was assessed using the alamarBlue™ assay following instructions given by the manufacturer. The quantity of DNA was then ascertained by PicoGreen® assay following the manufacturer's instructions.

3.9. Glucose-Responsive Fibrin Hydrogel

A glucose-responsive fibrin hydrogel (GRFHG) was fabricated in the following manner. Each GRFHG includes 100 µL (20 mg mL^{-1}) fibrinogen, GOx 100 ng, catalase 5 µg, and 20 µL of thrombin (100 U mL^{-1}). The gelation time for each of the hydrogels was 3–5 min.

3.10. Characterization of GRFHG

The glucose response to the fabricated GRFHG was determined by measuring the swelling properties. Glucose-responsive

Table 1. In vivo study design of the study (N = 8).

Treatments	1. PBS
	2. Fibrin hydrogel
	3. GRFHG
Types of animals	1. Diabetic
	2. Non-Diabetic
Timepoint	Seven Days
Wound:	Square (1 cm^2)

release of encapsulated material was also studied. Finally, the cytotoxicity of the GRFHG was assessed.

3.10.1. Degradation and Swelling of GRFHG

The conformational changes of GRFHG in the presence of glucose have been studied. Fabricated GRFHG was incubated with different concentrations of glucose, i.e., 0, 100, and 400 mg dL^{-1}. The reduced pH of the medium due to the production of gluconic acid was measured with a pH meter. After applying various glucose concentrations, the increased or decreased hydrogel size was photographed and compared within the different groups. The quantification of the swelling was carried out by weighing each of the hydrogels.

The microscopic technique determined glucose-responsive delivery of loaded FCPMCs. 1,00000 FCPMCs were encapsulated within the GRFHG at the time of fabrication. Various glucose concentrations (0, 100, 400 mg dL^{-1}) were added to FCPMC encapsulated GRFHG. After 48 h of incubation, the supernatant released from the gel was analyzed for the presence of FCPMC. A hemocytometer counted the number of FCPMCs released from the GRFHG under the microscope.

3.10.2. Cytocompatibility of GRFHG on NHEK

The ability of the GRFHG to preserve the metabolic activity of NHEK was assessed using the alamarBlue™ cell metabolic activity assay following the manufacturer's instructions. Briefly, 10 000 cells were seeded onto the top of GRFHG in a 96 well plate. After incubation of 48 h, the supernatant was removed from the well with a pipette and replaced with a 10% alamarBlue™ solution in each of the wells for 4 h. The intensity of the solution from the different treatments was determined with a spectrophotometer. A non-glucose-responsive fibrin hydrogel was used as a positive control.

3.11. The Glucose-Responsive Dual Nucleic Acid Delivery System in db/db Mouse

In vivo efficacy of the developed system for responsive nucleic acid delivery was assessed in a genetically diabetic db/db mouse model (**Table 1**). A genetically diabetic mouse BKS.Cg-*Dock7m* +/+ *Leprdb*/J of age 8–10 weeks were obtained from Charles River UK Ltd. Under anesthetic, surgical procedures on these mice were performed. The mouse's dorsal surface was shaved,

made sterile and draped for aseptic surgery. Two 10 mm^2 square excisional wounds on the dorsal side of each animal were created with a scalpel and scissors. Two square-shaped splints were placed bilaterally at the designated locations, and the splint was fixed to the skin by suturing the corners to stabilize the position.

The developed glucose-responsive dual nucleic acid delivery system was topically applied to the wound. The system was loaded with two reporter nucleic acids, i.e., GFP and GLuc. The wound created by the excision was filled with 200 μL of the treatment. A trimmed plastic cover dressing (Tegaderm™/Bioclusive™ Film) was placed on the splint. To prevent dressing loss or to prevent the mouse from biting the wound or being bitten by its cage mates, a protective jacket made from bandages and adhesive tapes was applied to the wound area. Wound-related complications were evaluated on the third-day post-surgery. Animals were euthanized on day seven by intraperitoneal sodium pentobarbital injection at 150 mg kg^{-1}. The wound area was excised for subsequent reporter gene expression, wound investigation, and histology.

3.12. Tissue Compatibility

The sections of 5 mm thickness was cut by using microtom. The excised wound tissues were formalin-fixed and embedded in paraffin. The slides were stained with masson's trichrome staining using a standard protocol. A check was made any undesired signs, i.e., inflammation of the fabricated system.

3.13. Glucose-Responsive Nucleic Acid Delivery

Glucose responsive dual gene delivery system was tested in in vivo genetically diabetic mice model. Two report genes, i.e., GFP, GLuc have been successfully delivered to the mice tissue through the fabricated delivery system. The paraffin-embedded skin sections were observed under an inverted fluorescence microscope to spot the GFP-positive cells. In case of GLuc, the snap frozen skin tissues were homogenized in 200 μL of cell lysis buffer in a homogenizer with beads for 2 h at 4 °C. The homogenate was centrifuged at 10 000 r min^{-1} for 10 min. 20 μL of the supernatant was collected, and a luciferase assay was carried out using a standard luciferase assay.

3.14. Glucose-Responsive Dual Nucleic Acid Delivery in Db/Db Mouse

The in vivo efficacy of the responsive nucleic acid delivery system has been assessed in a genetically diabetic db/db mouse model. A genetically diabetic mouse, BKS.Cg-*Dock7m* +/+ *Leprdb*/J of age 8–10 weeks were obtained from Charles River UK Ltd Animals were allowed to acclimatize for at least seven days before any surgical procedure was conducted. The dorsal surface of the mouse was shaved, prepared in a sterile manner, and draped for aseptic surgery. Two 10 mm^2 square excisional wounds on the dorsal side of each animal were created with the help of a scalpel and scissors. Two square-shaped splints were placed bilaterally at the designated locations, and the splints were fixed to the skin

**ADVANCED
SCIENCE NEWS**

www.advancedsciencenews.com

**ADVANCED
BIOLOGY**

www.advanced-bio.com

by suturing the corners to secure them. The glucose-responsive dual nucleic acid delivery system was topically applied to the wound. The system was loaded with two reporter nucleic acids, i.e., GFP and GLuc. The injury created by the excision was filled with 200 µL of the treatment. A trimmed plastic cover dressing (Tegaderm™/Bioclusive Film) was placed on the splint. To prevent dressing loss or to prevent the mouse from biting the wound and being bitten by its cage mates, a protective jacket made from bandages and adhesive tape was applied to the wound area. After seven days, the wound area was excised for subsequent wound investigation and histological analysis. Wound-related complications were evaluated on the third-day post-surgery. Animals were euthanized after day seven by intraperitoneal injection of sodium pentobarbital at 150 mg kg^{-1} dose.

3.15. Wound Closure Measurements

Digital images of the wound were analyzed for wound closure using Image J, Image J, National Institutes of Health (NIH), USA. The scale of measurement was set using the known distance in the image. The area of each wound was measured. The wound closure was then calculated by using Equation 1:

$$\% C = \frac{A_0 - A_i}{A_0} \times 100 \tag{1}$$

where % C = Percent closure, A_i = Area of the wound on the day of sacrifice, A_0 = Area of the wound at day zero.

3.16. Histology and Immunohistochemistry

The sections were formalin-fixed and embedded in paraffin. The sections were then cut in 5 mm thicknesses. The sections were saved from the block when the tissue was reached in the block. This ensured that all sections were saved at the cross-section of the wound. Slides were stained with Masson's trichrome staining using a standard protocol.

3.17. Stereology

Trichrome-stained slides were captured at 20X magnification of the slide scanner (Olympus digital slide scanner VS120FL). Each section was divided into ten parts, and the wounded area was used for stereology analysis. Standard stereological methods of our lab were used to do the stereological study. The volume fraction of inflammatory cells was measured using a 192-point grid. Blood vessels' surface and length density were measured using a cycloidal line grid.

3.18. Inflammation

Stereology analysis determined the number of inflammatory cells observed in the wounded tissue site. Volume fraction (V_V) is best estimated by point counting. Intersecting grid points (P_P) were counted for neutrophil and macrophage cells. This Pp was divided by the total grid points for each field of view (P_T). From

three fields of view on each section, a cumulative volume fraction of inflammatory cells was calculated using Equation 2.

$$V_V = \left(\frac{P_P}{P_T} \right) \tag{2}$$

3.19. Angiogenesis

The following methodology measured angiogenesis in the wounded tissue. Each field of view was overlaid by a cycloidal grid of 40 microns radius. The grid consisted of five test lines, each line comprising 58 cycloid arcs. The combined length (L_T) of cycloid arcs was 11 600 mm. The number of times a blood vessel intersected (I) with an arc was investigated, and the surface density (S_V) was calculated using Equation 3.

$$S_V = 2 \times \frac{1}{L_T} \tag{3}$$

Each captured field of view was rotated by 90 degrees to measure the length density of blood vessels. As described above, the cycloidal grid was placed in the same orientation. Blood vessel (I) and test line intersections were counted, and the length density (Lv) of blood vessels was calculated by using Equation 4, in which (T_S) is the thickness of the section and (L_T) is the total length of the test line.

$$L_V = \frac{2 \times I}{L_T \times T_S} \tag{4}$$

Radial diffusion distance (R_{diff}) between the blood vessels was calculated using Equation 5.

$$R_{diff} = \frac{1}{\sqrt{\pi \times L_V}} \tag{5}$$

3.20. Immunohistochemistry

The potential therapeutic effect of the developed GRFHG was determined by immunohistochemistry on the GRFHG-treated mice wound tissue. Blood vessels were identified by the cluster of differentiation 31 (CD31) marker, and inflammation was recognized with the marker cluster of differentiation 68 (CD68). Identification of blood vessels was confirmed by immunohistochemistry with endothelial cell marker CD31 using the manufacturer's standard protocol. Briefly, at 37 °C enzymatic antigen retrieval was carried out using 1X proteinase K (20 µg mL^{-1}, Sigma–Aldrich) solution in Tris-EDTA (TE) buffer (50 mM Tris Base, 1 mM EDTA, pH 8.0, Sigma–Aldrich). Primary rabbit polyclonal to CD31 (Anti-CD31 antibody: ab28364)) (1:100 in 0.01 M PBS containing 1% BSA) antibody was used with an overnight incubation at 4 °C. The sections were incubated with Alexafluore 546 secondary antibodies at 1:250 dilution in PBS with 1% BSA for 2 h, then washed with PBST before counterstaining with 4,6-diamidino-2-phenylindole (DAPI) (1:1000 in PBS) for 5 min.The following immunohistochemistry protocol was used to determine inflammation in the skin tissues. Briefly, enzymatic

antigen retrieval was carried out at 37 °C using a 1X proteinase K (20 mg mL^{-1}, Sigma–Aldrich) solution in Tris-EDTA (TE) buffer (50 mM Tris Base, 1 mM EDTA, pH 8.0, Sigma–Aldrich). Primary rabbit polyclonal to CD68 (Anti-CD68 antibody: ab28364)) (1:300 in 0.01 M PBS containing 1% BSA) antibody was used, with an overnight incubation at 4 °C. The sections were incubated with Alexafluore 546 secondary antibodies at 1:250 dilution in PBS for 2 h, washed with PBST and counterstained with DAPI (1:1000 in PBS) for 5 min.

3.21. Proteomics

Approximately 50 mg of snap-frozen tissue was homogenized in 1 mL of 8 M urea buffer in a tissue homogenizer (Tissue LyserLT, Qiagen) with beads at 4 °C for 2 h. Then the homogenate was centrifuged at high speed for 10 min, and the supernatant was collected. Following this, the extracted protein samples were trypsin digested and purified. The extracted protein samples were run on a Thermo Scientific Q Exactive mass spectrometer connected to a Dionex Ultimate 3000 RSLC nano chromatography system. Raw mass spectrometry (MS) data were analyzed with MaxQuant software based on specified peptides with unspecified enzymatic cleavage for proteinase K-digested samples and semi-specific samples to quantify the identified proteins trypsin cleavage with fixed modification of carboxymethylation for tryptic samples. Each peptide used for protein identification and quantification met specific MaxQuant parameters: only peptide scores corresponding to a false discovery rate (FDR) of ≤1% were accepted from the MaxQuant database search. Perseus software was used for further comprehensive proteomics data analysis, including label-free quantification of the identified proteins. T-test p-value 0.05 filter valid values – must be observed in all three replicates of at least one group. The protein expression comparison between the no treatment and the GRFHG hydrogel groups was conducted using an empirical test based on fold change value.

3.22. Validation of the Target

To validate the proteomic data (**Table 2**), the immunohistochemical staining of highly regulated markers, i.e., Alpha-actinin-2 (Actn2), desmin, myosin binding protein-C 1 (MYBPC1), were studied. The sections were then formalin-fixed and embedded in paraffin. The tissue sections were then cut into 5 mm thicknesses. For immunohistochemistry, the sections were incubated with proteinase K for 20 min at 37 °C, followed by 1% (w/v) BSA for 30 min at room temperature before overnight incubation at 4 °C with primary antibodies. Negative control sections were incubated with PBS and washed in PBST. Staining was performed with three selected primary antibodies in three different reactions (1:200 Actn2: Abcam-Ab9465), desmin (1:100 Santa Cruz Biotechnology sc-23879), MYBPC1 (1:200, Protein Tech (22900-1-AP,) per section. The sections were incubated with Alexafluor 546 secondary antibodies at 1:250 dilution in PBS for 2 h, then washed with PBST, followed by counterstaining with DAPI (1:1000 in PBS) for 5 min. All slides were cured at 4 °C in the dark for 24 h before imaging with an inverted fluorescence microscope/slide scanner. Three parts of the divided section were used to analyze each marker per animal. Slide scanner microphotographs were converted to binary mode (8 bit) and adjusted to the optimal threshold of positive staining and total area. Area fraction (Vv) was calculated by quantifying the area fraction of the positively stained matrix component divided by the total area and converting it into a percentage (%) as below:

Table 2. Initial screening of up or downregulated proteins in the GRFHG treatment group as compared to the no-treatment group.

Proteins	Intensity Log$_{10}$ [No treatment]	Intensity Log$_{10}$ [GRFHG]	Normalised Fold change	Up/Downregulated
Alyref	7.744259073	7.637809829	1.27775987	↓
Sfn	9.419278188	8.757944881	4.584936312	↓
Hsp90b1	7.974235277	7.845079427	1.346343415	↓
Tpi1	9.297103659	9.750544397	2.840800509	↑
Eno3	8.469502933	9.000137516	3.393396309	↑
Fkbp1a	8.026042721	8.002556247	1.055568627	↓
Des	8.960719642	9.49106274	3.391119526	↑
Dbi	9.822222583	9.681455313	1.382825151	↓
Slc25a4	7.625559373	8.212143196	3.859969054	↑
Hnrnpk	8.927397741	8.710557363	1.647556733	↓
Rps23	7.816782449	8.398136835	3.813769011	↑
Dynlrb1	8.004149342	8.03686567	1.078242208	↑
Atp5a1	8.708876783	9.118551295	2.568470085	↑
Ddx5	7.57170107	7.52505345	1.113390778	↓
Hspe1	9.274673463	9.065181211	1.619915093	↓
Rps19	7.17079936	7.784850185	4.111978405	↑
Atp5o	8.114899973	8.491123474	2.378063798	↑
Prkar1a	8.079362164	7.929854705	1.410936472	↓
Actn2	7.395442888	8.165669606	5.891511332	↑
Dstn	8.327815141	8.234559462	1.239526107	↓
Krt16	9.22999139	7.419509666	64.63707928	↓
Pabpc4	7.848061787	8.122390653	1.880740453	↑
Mybpc1	7.549534559	8.043178827	3.116335935	↑

$$\text{Percentage area fraction} \left(\%V_V \right) = \frac{\text{Area Fraction} \times 100}{\text{Total Area}} \qquad (6)$$

3.23. Glucose-Responsive H$_2$O$_2$ Production

GOx reacts with glucose to form gluconic acid and a by-product, H$_2$O$_2$. We have quantified glucose-responsive production of H$_2$O$_2$ from the developed GRFHG in vitro in the presence of different glucose concentrations.

The quantification of H$_2$O$_2$ produced was estimated using a fluorometric hydrogen peroxide assay kit (MAK165-1KT-Sigma–Aldrich) as per the manufacturer's instructions. The master mix was prepared by adding red peroxidase substrate Stock (50 µL), peroxidase stock (200 µL), assay buffer 4.75 mL. Then, 50 µL of the master mix was added to each of the wells (samples, standards, and controls). This was then mixed well, and the plate was incubated at room temperature for 15–30 min. The plate was then protected from light during the incubation. Finally, a fluorescence plate reader measured the fluorescence intensity at (lex

ADVANCED
SCIENCE NEWS
www.advancedsciencenews.com

ADVANCED
BIOLOGY
www.advanced-bio.com

= 540/ lem = 590 nm). The production of H_2O_2 was determined at three time points: 10, 60, and 90 min.

4. Statistical Analysis

All statistical analyses were done using GraphPad Prism® 6.00 software, Inc. Data were analyzed by one-way analysis of variance (ANOVA) followed by Tukey or Dunnett's or Bonferroni multiple comparison test(s). $p < 0.05$ was statistically significant.

5. Animals

All animal-related protocols were performed following the national guidelines and approved by the Animal Care Research Ethics Committee (ACREC) at the National University of Ireland, Galway, and the Health Product Regulatory Authority (HPRA) Ireland. A genetically diabetic mouse BKS.Cg-*Dock7m* +/+ *Lep-rdb*/J of age 8–10 weeks was obtained from Charles River UK Ltd.

5.1. Surgical Procedure

Two 10 mm² square excisional wounds on the dorsal side of each animal were created with the help of a scalpel and scissors. Two square-shaped splints were placed bilaterally at the designated locations, and the splint was fixed to the skin by suturing the corners to stabilize the position. Treatments (200 µL) were topically applied on the wounds' surface and then covered with a Tegaderm™ dressing. A protective jacket, dressings, and adhesive tape was used to cover the area of surgery. The animals were euthanized seven days post-surgery by intraperitoneal injection of sodium pentobarbital at 150 mg kg⁻¹ dose. The wound area was excised and then fixed in formalin for histological and immunohistochemical analysis.

6. Results

6.1. Morphological, Chemical Characterization of FCPMC

The $CaCO_3$ sacrificial template was first synthesized by colloidal crystallization from a supersaturated solution. The fabrication of FCPMCs was achieved through the LbL approach. Different polyelectrolytes have been coated on the $CaCO_3$ template by electrostatic interaction. **Figure 2**G–J, shows scanning electron microscopy (SEM) images of the various steps involved in the synthesis of FCPMC. The FCPMCs formed were monodispersed and spherical. The surface charge after each coating ranged from +30 mV to −30 mV (Figure 2A). After each coating, the charge shifted from positive to negative and vice versa, ensuring that each layer was successfully coated.

The average size of fabricated FCPMCs determined with the zeta sizer was between ≈2900 and 3100 nm (Figure 2C). The overall charge on the surface of FCPMCs was −18.5 mV (Figure 2D). The presence of fibrin in FCPMCs was confirmed by inverted microscopy analysis, shown in Figure 2B. Complete removal of the $CaCO_3$ template from the FCPMC was confirmed with TEM and EDX analysis (Figure 2E,F). A TEM image of FCPMC is shown in Figure 2E, and the complete hollowness in the central region suggests that no template remained after EDTA treatment. Complete template removal from the FCPMC is confirmed by EDX analysis (Figure 2F).

FCPMC were loaded with Cy3 labelled GFP polyplex by diffusion (**Figure 3**A). The Cy3 labelled GFP polyplexes were confirmed by observation using an inverted microscope under the Texas red channel. The loaded polyplexes were ≈90%, suggesting that the fabricated FCPMCs have excellent encapsulation capacity (Figure 3B). The release kinetics of the encapsulated polyplex was assessed using a spectrophotometer. Around 120 ng of polyplex was released from the FCPMC after 350 h of incubation (Figure 3C). This showed that the delivery system could release a payload over a longer period, giving a more extended therapeutic benefit.

6.2. Cytocompatibility of FCPMC

Cytocompatibility of FCPMC on normal human keratinocytes (NHEK) cells were analyzed by alamarBlue™ cell metabolic activity assay and live and dead assay.

6.2.1. alamarBlue™ cell Metabolic Activity Assay

Different amounts of FCPMs, ranging from 50 000 to 1 000 000, were incubated with normal human keratinocytes (NHEK) cells for 24 and 48 h. In the presence of FCPMC at its highest concentration, the cells did not show changes in metabolic activity after 24 or 48 h of incubation (Figure S1A, Supporting Information). This confirmed that there was no cytotoxicity associated with FCPMC.

6.2.2. Live and Dead Assay

Live dead assay has been conducted to establish that cells are not dying in the presence of FCPMC. Under an inverted microscope, no dead cells were observed in the FCPMC-treated group, even at the highest concentration after 48 h of incubation (Figure S1B, Supporting Information).

6.3. Optimization of Plasmid: Polymer Ratio for GLuc

Different plasmid: polymer ratios were used to complex the gLuc plasmid. As shown in Figure S2C (Supporting Information), 1:7 and 1:20 concentration of the polymer could entirely complex gLuc. However, only the 1:20 concentration showed successful transfection (Figure S2D, Supporting Information).

6.3.1. Optimization of the Plasmid: Polymer ratio for GFP

As with GLuc, plasmid 1:20 ratio was the optimal polymer concentration (Figure S2A,B, Supporting Information).

6.3.2. Optimization of GLuc Polyplex Dose in Keratinocytes

A range of doses from 1–25 µg was used to transfect keratinocytes (Data not shown). Higher doses of 5–25 µg of polyplexes were
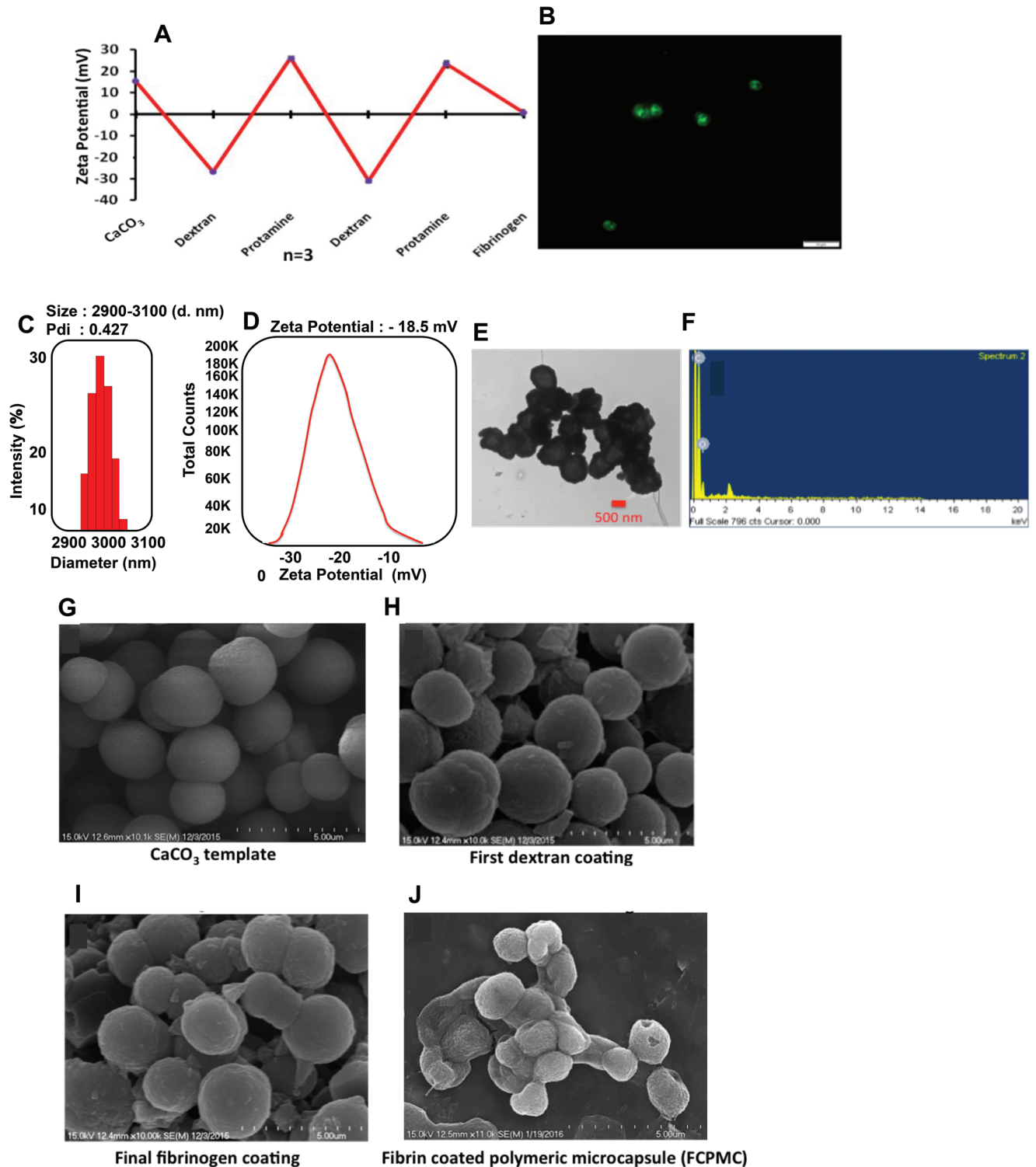
**ADVANCED
SCIENCE NEWS**

www.advancedsciencenews.com

**ADVANCED
BIOLOGY**

www.advanced-bio.com

Figure 2. Characterization of FCPMC A) Surface charge after each polyelectrolyte coating on the CaCO$_3$ template B) Top FITC-labelled fibrin layer of FCPMC. Scale bar = 10 µm C) Average diameter size, polydispersity index (PDI) of FCPMC D) Surface charge on the surface of FCPMC E) Transmission electron microscopy (TEM) image of FCPMC. Scale bar = 500 nm F) Energy-dispersive X-ray (EDX) spectrum of FCPMC after CaCO$_3$ removal. G) Scanning electron microscopy (SEM) image of only CaCO$_3$ template H) scanning electron microscopy (SEM) image after first dextran coating I) SEM image last fibrinogen coating J) SEM image of the final product. Scale bar = 5 µm.
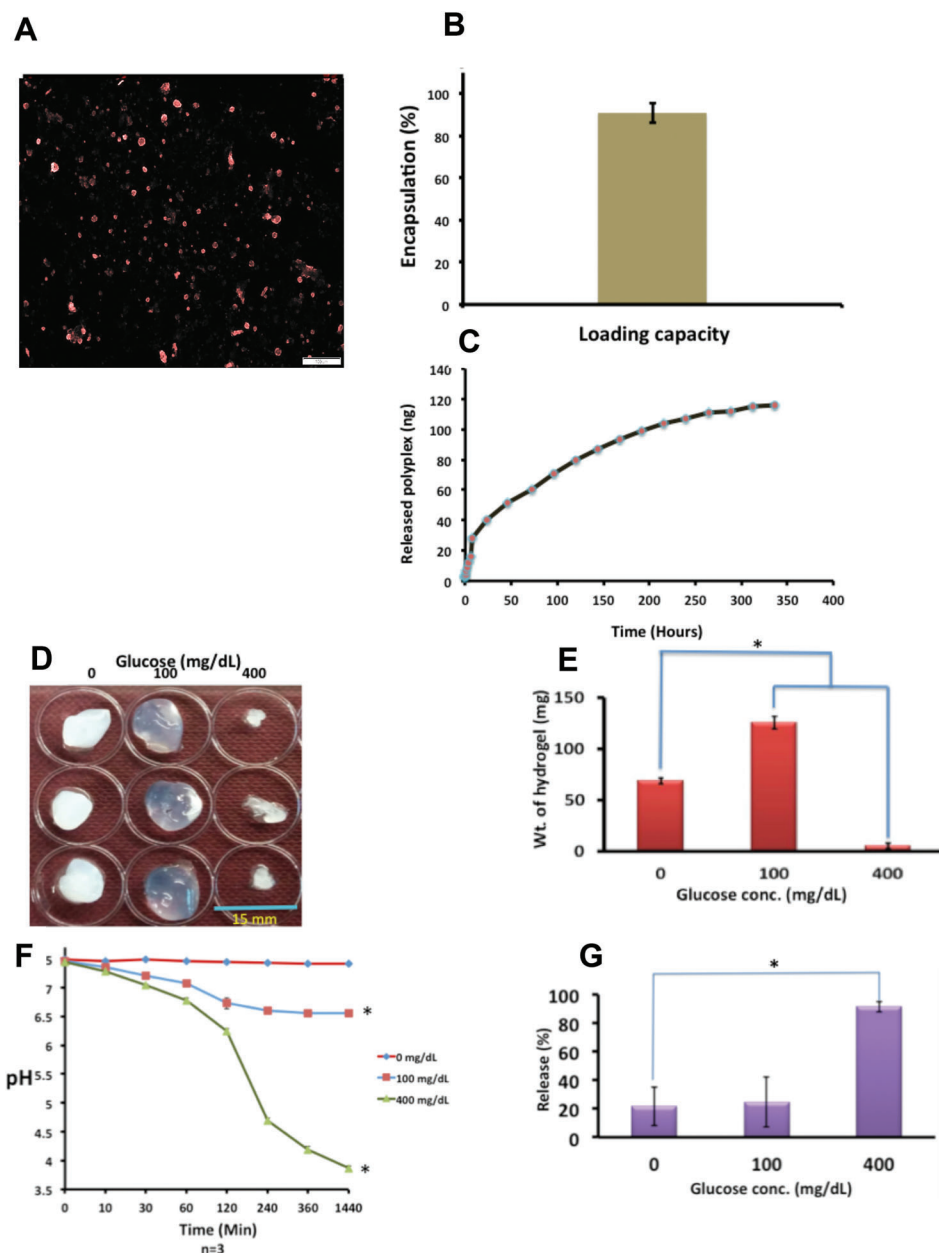
**ADVANCED
SCIENCE NEWS**

www.advancedsciencenews.com

**ADVANCED
BIOLOGY**

www.advanced-bio.com

Figure 3. A) Fluorescence image of Cy3 labelled polyplex encapsulated within FCPMC Scale bar = 200 μm B) Polyplex encapsulation capacity C) Release of polyplexes from FCPMC, n = 3, SD, D) GRFHG swelling in the presence of glucose, Scale bar = 15 mm E) Weight changes in GRFHG with the presence of glucose * represents statistical significance by One-Way ANOVA F) pH reduction in the presence of glucose. * Represents statistical significance by Two-Way ANOVA (Bonferroni post hoc test) G) Responsive delivery of FCPMC from GRFHG, * represents statistical significance by One-Way ANOVA, n = 3, SD, p < 0.05.

toxic to the NHEK cells. Therefore, a lower concentration of polyplexes, i.e., 1 μg, was used to transfect NHEK cells. At 1 μg concentration, a higher transfection was observed (4×10^7). The highest metabolic activity and DNA content were observed at 1 μg concentration (Figure S2G, Supporting Information).

6.3.3. Optimization of GFP Polyplex Dose in Keratinocytes

A similar series of experiments were carried out for GFP to find the optimal dose. GFP-expressing cells, metabolic activity, and

PicoGreen® assay confirmed that (a) 1 μg dose of GFP plasmid was optimal for the keratinocytes (Figure S2E,F, Supporting Information).

6.4. Glucose-Responsive Fibrin Hydrogel

GRFHG has been successfully fabricated by using the enzyme GOx. When glucose reacts with GOx, it produces gluconic acid and increases the proton concentration in the medium. The

generated protons protonate the amines that are present on the fibrin surface. This interaction makes conformational changes in hydrogel morphology and facilitates water absorption at a high glucose level, leading to the hydrogel's swelling. After continuous exposure, this water pressure becomes high enough to disrupt the hydrogel integrity. The average weight of GRFHG is ≈75 mg. When normoglycemic glucose concentration (100 mg dL^{-1}) was applied to the GRFHG, the weight increased due to water intake up to 120 mg. However, at a higher glucose concentration (400 mg dL), the weight was reduced to 10 mg. The reduction in the weight was due to the burst release from hydrogel because of water pressure that was too high (Figure 3D,E). The altered pH of GRFHG in the presence of 0, 100, and 400 mg dL^{-1} glucose was determined with a pH meter at several time points. Figure 3F shows a reduction of pH among different experimental groups. At 0 mg dL^{-1} glucose, there was minimal change in the initial pH. However, in the case of 100 mg dL^{-1} glucose, the pH reduced from 7.4 to 6.5.

Moreover, a substantial pH change occurred at a higher glucose concentration (400 mg dL^{-1}), reducing the pH to four. The primary purpose of GRFHG synthesis was to develop a glucose-responsive platform to deliver therapeutic biomolecules. To determine the ability of GRFHG to deliver a payload depending on glucose concentration, synthesized FCPMC were encapsulated within the GRFHG. In the case of 0 mg dL^{-1}, ≈20% of FCPMC was released in the medium. At 100 mg dL^{-1} glucose concentration, the release of FCPMC was also 20%. When 400 mg dL^{-1} of glucose was applied, ≈90% of FCPMC was released (Figure 3G). This experiment confirmed that the fabricated system is glucose-responsive and can deliver a payload proportionate to the glucose concentration.

6.5. Cytocompatibility of GRFHG

Cytocompatibility of GRFHG was analyzed with alamarBlue™ cell metabolic activity assay. The cells inoculated on top of the GRFHG did not show any reduction in metabolic activity compared to fibrin hydrogel. The cells seeded on top of the GRFHG showed a slightly higher metabolic activity at both time points used for the study. This study suggests that the cell metabolic activity was not altered in the presence of GRFHG (Figure S1D, Supporting Information).

6.6. In Vivo Tissue Compatibility

Using a scalpel and scissors, two 10 mm^2 square wounds were created on the dorsal side of the mice. The wound tissues of GRFHG-treated mice were analyzed for any undesired changes. The results showed no tissue toxicity associated with the treated animals. No signs of fibrosis were observed in any of the treatment groups (Figure S1E, Supporting Information).

6.7. Glucose-Responsive Nucleic acid Delivery

The harvested skin tissue of the genetically diabetic mice showed increased reporter gene expression. An increased GFP expression has been observed in the tissue of the GRFHG treatment
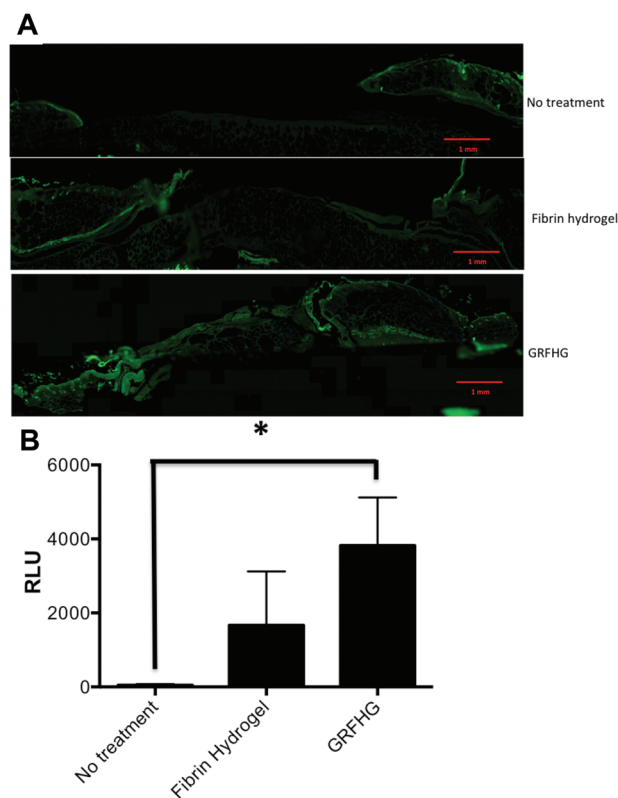

Figure 4. Glucose-responsive dual nucleic acid delivery in vivo A) GFP expression in diabetic mice, the scale bars represent 1 mm B) Glucose-responsive GLuc expression in diabetic mice skin post GRFHG treatments.

group animals under green fluorescence. Additionally, the intensity of the second gene of interest, i.e., GLuc, was maximum among the treatment groups, which was 4000 RLU (**Figure 4**).

6.8. Wound Closure

The mice treated with the developed system were sacrificed seven days after surgery, and the harvested wound tissues were used to analyze wound healing parameters like wound closure and angiogenesis. Around 20% of wound closure occurred in the non-treatment group, whereas in the GRFHG treatment group, more than 60% of the wound was closed (**Figure 5**A,B). GRFHG significantly improved diabetic wound healing compared to the no-treatment group after seven days post-injury. In non-diabetic mice, treatment of GRFHG was also able to improve wound closure. As these are non-diabetic animals, higher wound closure was observed in the no-treatment group, i.e., ≈40% (Figure 5A,B). In the GRFHG-treated mice, more than 60% of the wound was closed. However, this increased wound healing in the GRFHG treatment group was not significant. The fact that we were able to treat diabetes wounds at the same rate as non-diabetic wounds indicates a good result and motivates us to pursue further options that this technology may provide. In vivo assessment suggested that the system increases healing in diabetic and non-diabetic animals.
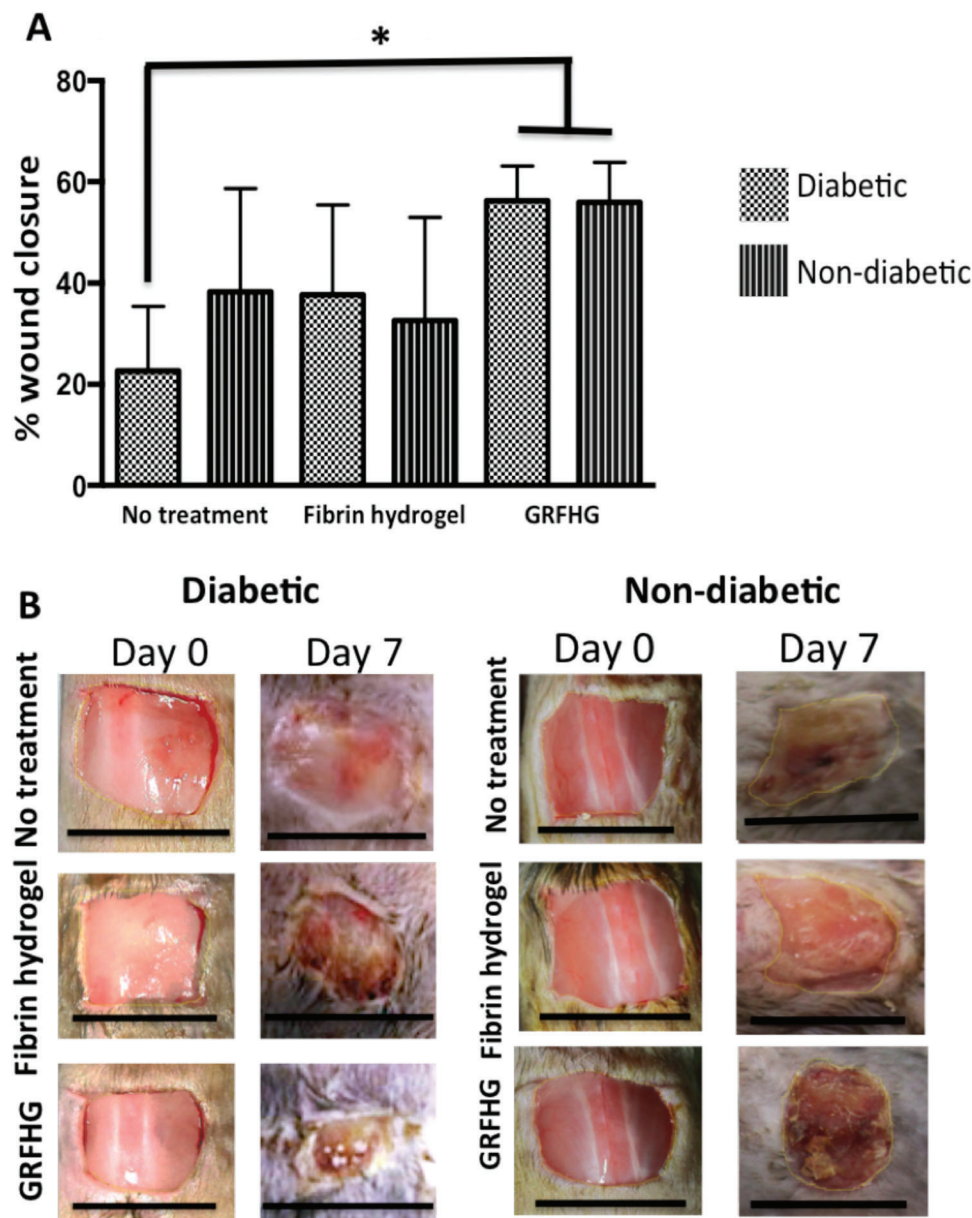
**ADVANCED
SCIENCE NEWS**

www.advancedsciencenews.com

**ADVANCED
BIOLOGY**

www.advanced-bio.com

Figure 5. The treated wounds were digitally photographed post-surgery. The wound area was determined using software ImageJ in db/db mice A) % Wound closure B) Representative images of wound closure. * Represents statistical significance by One-Way ANOVA, Dunnett's multiple comparison tests, $n = 5$, scanning electron microscopy (SEM), $p < 0.05$, The scale bars represent 1 cm.
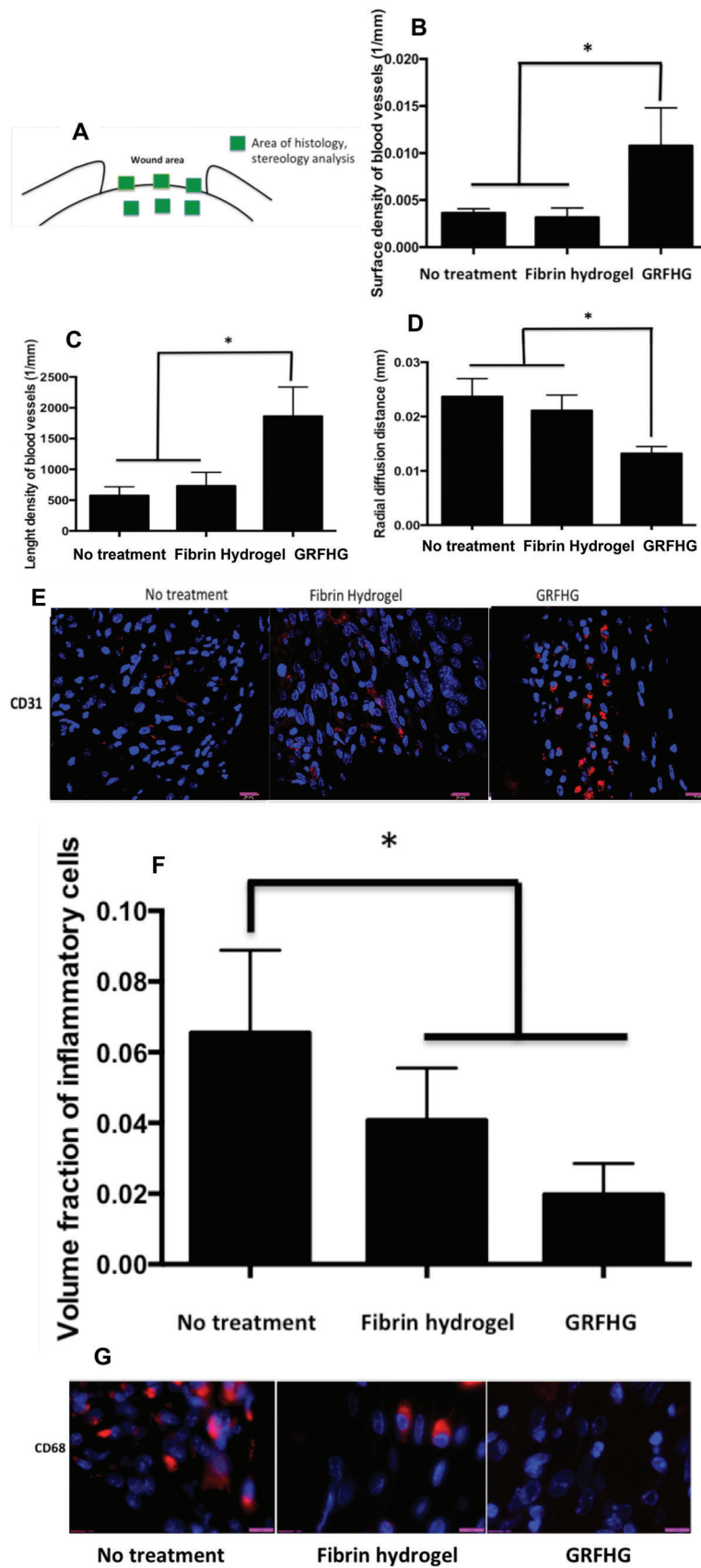
6.9. Tissue Response

Images of Masson's trichrome-stained slides were taken on the slide scanner at 20X magnification. Trichrome-stained tissues showed higher reepithelialization in the GRFHG treatment groups in diabetic and non-diabetic animals (**Figure 6** and Figure S3C,F, Supporting Information).

6.10. Proteomics

Proteomic analysis was done to screen the fundamental differences between no treatment and GRFHG treatment group in the tissue of db/db diabetic mice after seven days post-surgery. Also, from this analysis, biomolecules that were involved in wound healing were identified. A total of 23 proteins were significantly altered between the no treatment versus GRFHG treatment group (Table 1). Actn2 is one of the critical proteins involved in wound healing whose expression was increased in the GRFHG treatment group. Actinin is closely linked with β-Actin, and actin is a crucial molecule in the management of cellular proliferation, adhesion, and migration, resulting in a tightly controlled equilibrium between tissue regeneration and fibrosis, thus contributing to the re-establishment of the skin barrier functions, restoration of the skin anatomical structure and wound repair. As per

**ADVANCED
SCIENCE NEWS**

www.advancedsciencenews.com

**ADVANCED
BIOLOGY**

www.advanced-bio.com

2300161 (13 of 18)   © 2023 The Authors. Advanced Biology published by Wiley-VCH GmbH

**ADVANCED
SCIENCE NEWS**

www.advancedsciencenews.com

**ADVANCED
BIOLOGY**

www.advanced-bio.com

protein data from MS analysis, Actn2 was the most upregulated biomolecule in the GRFHG treatment group. Actn2, along with two other protein biomolecules, i.e., desmin and MYBPC1, were observed in the protein dataset and as IPA upstream regulators as well. Upstream regulators are important because they can influence the expression of other proteins. To confirm increased expressions of Actn2, desmin, and MYBPC1 in the GRFHG treatment group, we have validated the expression of these proteins by immunohistochemistry analysis (**Figure 7**).

6.11. Glucose-Responsive H_2O_2 Production

The highest amount of H_2O_2, ≈9 µM, was generated in GRFHG treatment in vitro (Figure 8A,B). Proposed mechanism of the therapeutic glucose-responsive fibrin hydrogel.

7. Discussion

A diabetic wound is a complex pathology of diabetes for which no definitive treatment is yet available. Because it has a complex pathology, treating a diabetic injury with a single nucleic acid therapy would, at best, be only moderately successful. An obvious solution is multiple nucleic acid therapy constructs to treat diabetic wounds. Recently delivery of keratinocyte growth factor (KGF) and IGF-1 genes showed beneficial effects resulting in increased reepithelialization, proliferation, and decreased apoptosis compared to single nucleic acid constructs.[17] A combination of VEGF-A and FGF-4 gene delivery significantly improved wound healing in mice.[18] In addition, a mixed dose of platelet-derived growth factor (PDGF) and IGF-1 gene delivery showed higher therapeutic potential than that of individual delivery of either nucleic acid.[19] Simultaneous delivery of Rab18 and eNOS genes resulted in increased wound healing in an alloxan-induced hyperglycemic preclinical ear ulcer model of compromised wound healing.[12] The diabetic wound microenvironment is very dynamic, i.e., proteases, inflammatory cells, and enzymes are in higher amounts. Most of the reported multi-nucleic acid delivery strategies described above are not stimulus-directed, thus offering limited nucleic acid delivery and efficacy. Our study explored glucose sensitivity as a stimulus to improve nucleic acid delivery, as this stimulus is at a higher concentration in the diabetic wound microenvironment. Most of the developed glucose-responsive delivery systems have been utilized to deliver insulin to control the level of blood glucose.[20–22] The delivery of insulin enables the lowering of blood glucose for a short period. Fibrin is a widely accepted biomaterial for clinical use and has been utilized to deliver growth factors, cells, peptides and nucleic acids.[23] Many growth factors, i.e., vascular endothelial growth factor (VEGF) and PDGF, have been incorporated into the fibrin carrier and successfully delivered to enhance

wound healing.[24,25] Non-angiogenic growth factors associated with wound healing, such as KGF[26] and epidermal growth factor (EGF),[27] have been explored for wound healing purposes. Efficacy in cell therapy using keratinocytes[28] and mesenchymal stem cells (MSC)[29] through the fibrin carrier to treat wounds has also been reported.

We have successfully developed a fibrin-based glucose-responsive spatiotemporal dual nucleic acid delivery system that can be used to deliver multiple therapeutic nucleic acids topically to the hyperglycemic environment. The system is made up of a combination of FCPMC and GRFHG. FCPMC, which are hollow and GRFHG together, provides plenty of space for the payload. The FCPMCs fabricated by the LbL approach were 3 µm in size. Hollow capsules offer a higher payload capacity than self-assembled particles.[30] This is the first report describing fibrin hollow capsule synthesis and application. The fabricated FCPMCs are biodegradable, with a polyplex loading capacity of ≈90%. The encapsulated polyplexes were released from the FCPMCs slowly over an extended period.

A delivery system made up of fibrin gives additional benefit in the case of wound healing as it is an extracellular matrix (ECM) component. The addition of fibrin will organise ECM in a better way and help in wound healing.[31] A novel glucose-responsive fibrin hydrogel has been fabricated by adding a GOx enzyme. The GRFHG did not show any adverse effect(s) on cellular metabolic activity.

Furthermore, GRFHG showed glucose-responsive behavior through swelling in the presence of glucose. The release of the payload depends on the glucose concentration. Moreover, the combined system is cytocompatibility and tissue-compatible, which is expected to have a potential therapeutic effect on wound healing. In addition, the fabricated system itself acts as a therapeutic intervention as increased angiogenesis in the genetically diabetic db/db mice model was seen.

Additionally, treatment of the system reduced inflammation in the db/db mice. The system-treated group has shown upregulation of essential wound healing proteins, i.e., Actn2, desmin, and MYBPC1. Fibrin plays a crucial role in blood clotting, fibrinolysis, cellular and matrix interactions, inflammation, wound healing, angiogenesis, and neoplasia.[32] Besides this, fibrin is popular because of its biodegradability, non-toxic degradation products, flexibility in use, easy control over gelation, degradation, pore size, suitability for infiltration of host tissue, and a delivery vehicle simply by manipulating the concentrations of thrombin and fibrinogen.[31]

The proposed mechanism of wound healing by the action of GRFHG has been shown in **Figure 8**B and is described below. Glucose oxidase (GOx) is responsible for the glucose response in the fabricated system. GOx reduces the amount of glucose by converting it into gluconic acid, reducing hyperglycemia

Figure 6. Surface density, length density of blood vessels, and radial diffusion distance in the wounds A) Schematic representation of wound area chosen for histology and stereology B) On day seven post-surgery, the surface density in the GRFHG treatment group were significantly higher than that in the fibrin hydrogel and no-treatment control groups. C) On day seven post-surgery, the length density in the GRFHG treatment group was significantly higher than that in the fibrin hydrogel and no-treatment group D). The radial diffusion distance in the GRFHG treatment group was significantly reduced compared to that of the fibrin hydrogel and no-treatment groups E) Immunohistochemistry staining of angiogenesis marker CD31 in db/db diabetic mice with different treatment groups. The observed intensity of blood vessels was higher in the GRFHG treatment group F) Volume fraction of inflammatory cells G) Immunohistochemistry analysis of inflammation (CD68). The intensity of CD68, which represents inflammation, was reduced in the GRFHG treatment group. Scale bar = 10 µm *represents statistical significance by One-Way ANOVA, $n = 3$, SD, $p < 0.05$.

ADVANCED
SCIENCE NEWS

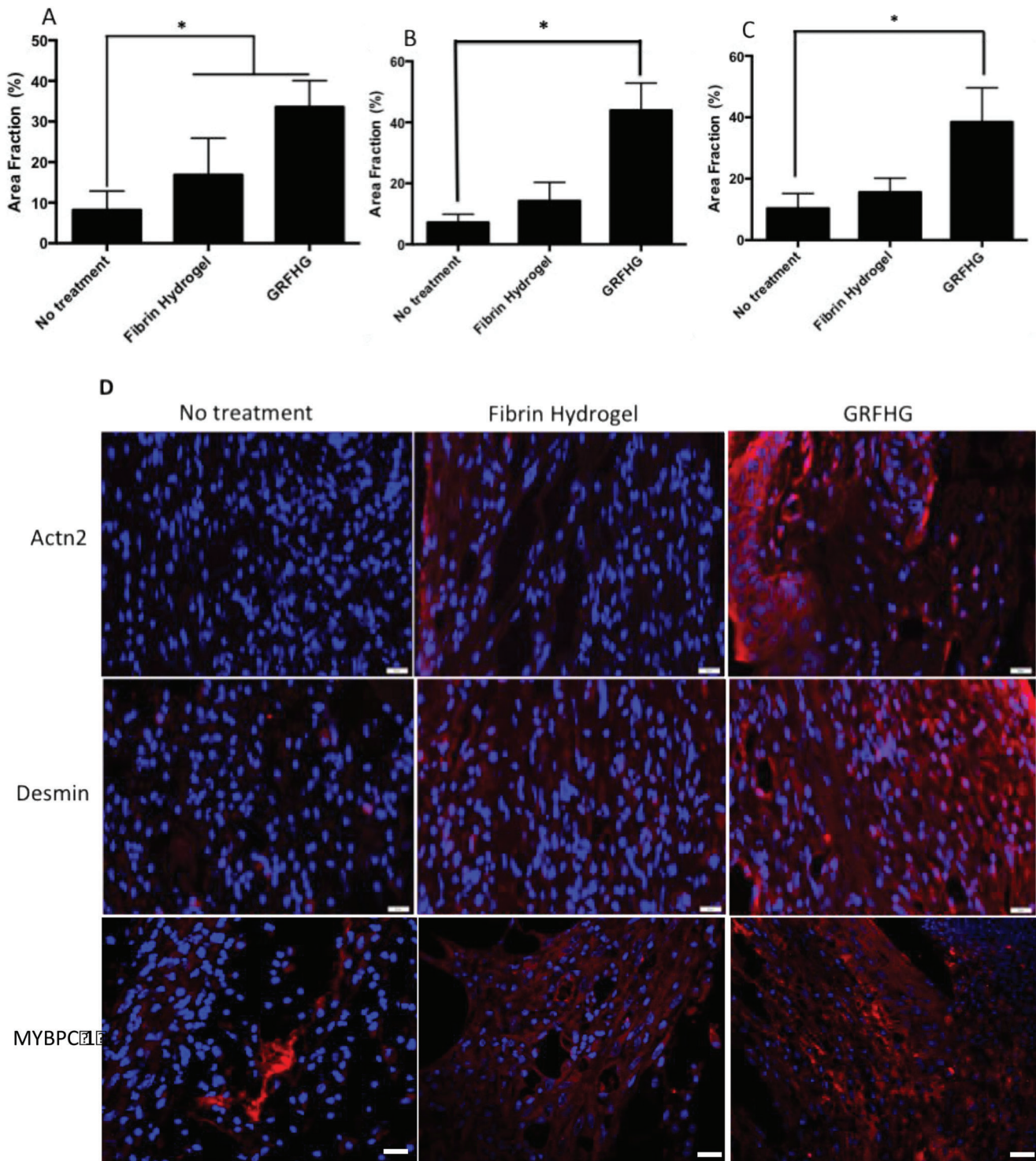www.advancedsciencenews.com

ADVANCED
BIOLOGY

www.advanced-bio.com

Figure 7. After seven days post-treatment, the volume fraction of positively stained cells in the wound tissue sections of genetically diabetic mice. A) Actn2 (Scale bar = 20 µm) B) Desmin (Scale bar = 20 µm) C) MYBPC1 (Scale bar = 20 µm) D) Representative images of validated targets. * Represents statistical significance by One-Way ANOVA, $n = 3$, SD, $p < 0.05$.
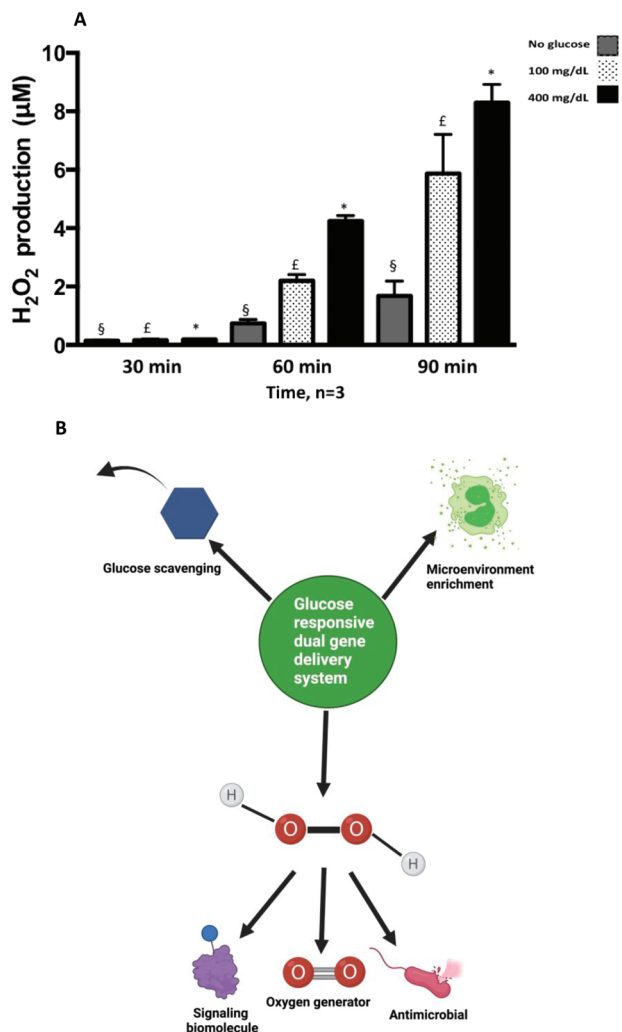
2300161 (15 of 18)

Figure 8. A) Glucose scavenging by Glucose oxidase (GOx), H$_2$O$_2$, as a secondary messenger and fibrin-mediated enrichment are essential factors proposed to participate in diabetic wound healing. B) Proposed mechanism of the therapeutic glucose-responsive fibrin hydrogel.

and related complications. Another advantage of GOx is that it produces small quantities of hydrogen peroxide as a by-product ($\approx$10 μM). The generated hydrogen peroxide can act as a secondary messenger,[33,34] antimicrobial,[35] and oxygen source after decomposition by catalase.[33] The recent evidence suggests possible therapeutic benefits of hydrogen peroxide in wound healing.[35,36] Also, hydrogen peroxide is relatively less reactive than other reactive oxygen species, allowing it to act as a signaling molecule.[37] Vukelic et al. showed that hydrogen peroxide modulates filamentous-actin binding, and this binding is a crucial step in wound healing.[38] Hydrogen peroxide delivers a "damage" message and stimulates effector cells to respond.[35] Hydrogen peroxide also activates mRNA expression of macrophage inflammatory protein-1α, macrophage inflammatory protein-2, and macrophage chemokine protein-1, which initiate the recruitment of phagocytes.[39–41] A scratch-wound model from keratinocyte cells showed that hydrogen peroxide promoted keratinocyte mobility at a low concentration of 500 μM.[42] It has been reported

that wound closure rate was significantly increased by the topical application of 10 mM hydrogen peroxide with a strong promotion of angiogenesis and connective tissue regeneration in a rat excisional wound model.[43] Also, hydrogen peroxide stimulates macrophages,[44] retinal keratinocytes,[45] and vascular smooth muscle cells[46] to release VEGF, which promotes angiogenesis. Hydrogen peroxide derived from the wounded skin cells of zebrafish strengthened injury-induced peripheral sensory axon regeneration.[47] Concentrations of hydrogen peroxide lower than 500 μM enhanced the release of heat shock protein and fibroblast growth factor from the cultured rat astrocytes, contributing to neuron survival, neurite outgrowth, and angiogenesis.[48]

In non-diabetic natural wounds, the healing rate is higher; with our GRFHG treatment, diabetic healing increases but less than in diabetic wounds. Therefore, we believe that diabetic and non-diabetic wounds showed no significant difference. It is a significant accomplishment that we were able to repair diabetes wounds at the same rate as non-diabetic wounds.

Despite the many advantages, there are a few limitations of this study. The amount of hydrogen peroxide produced from GRFHG by the action of GOx is limited and is good for wound healing. However, at higher glucose concentrations, an extra amount of hydrogen peroxide can be produced, which may have undesirable effects. Also, diabetic wound healing has a very complex pathology in which multiple microorganisms are growing and producing toxins. Additionally, in the diabetic wound, there is a presence of high levels of proteases, and these are prolonged unhealed wounds. However, in db/db diabetic wounds created on the backside of a mouse, the complications mentioned earlier could either not be produced or could not be considered in the study carried out. Furthermore, in the project, the comparison of protein array was done only between injury and treatment groups.

8. Conclusions

A dual nucleic acid delivery approach, i.e., glucose-responsive fibrin, has been established and exhibited an excellent responsive nucleic acid delivery capacity in an in vivo genetically diabetic db/db mouse model. Furthermore, the developed system does not show any undesired effects in vitro and/or in vivo. When applied to wounds in genetically diabetic db/db mice, the fabricated system increased reepithelialization and angiogenesis. The GRFHG system-treated mice tissue showed inflammation that was scaled down. Also, proteins involved in the wound healing process, i.e., Actn2, MYBPC1, and desmin, were upregulated in the GRFHG-treated group of animals; due to the generated H$_2$O$_2$. Taken together, the fabricated GRFHG has the potential to improve wound healing.

This system can also be encapsulated with multiple therapeutic nucleic acids, which will further aid wound healing. The developed system is compatible with cells and rodent tissues. While the results are impressive, this technology requires validation in other preclinical models to assess its potential and compatibility in humans.

Supporting Information

Supporting Information is available from the Wiley Online Library or from the author.

2300161 (16 of 18)

**ADVANCED
SCIENCE NEWS**

www.advancedsciencenews.com

**ADVANCED
BIOLOGY**

www.advanced-bio.com

Conflict of Interest

The authors declare no conflict of interest.

Author Contributions

A.P. performed conceptualization, experimental plans, supervised and funding acquisition, M.M. performed experimental plans, data curation and M.M. and R.B. wrote the manuscripts, A.S. performed data curation, A.L. edited the animal experiments. All authors have read and agreed to the published version of the manuscript.

Data Availability Statement

The data that support the findings of this study are available from the corresponding author upon reasonable request.

[1] X. M. Anguela, K. A. High, *Annu. Rev. Med.* **2019**, *70*, 273.

[2] Ö. Uğurlu, F. B. Barlas, S. Evran, S. Timur, *Plasmid* **2020**, *110*, 102513.

[3] C. C. Ma, Z. L. Wang, T. Xu, Z. Y. He, Y. Q. Wei, *Biotechnol. Adv.* **2020**, *40*, 107502.

[4] J. K. Venkatesan, A. Rey-Rico, M. Cucchiarini, *Tissue Eng Regen Med* **2019**, *16*, 345.

[5] M. Kulkarni, A. Breen, U. Greiser, T. O'Brien, A. Pandit, *Biomacromolecules* **2009**, *10*, 1650.

[6] M. Sato, E. Inada, I. Saitoh, S. Watanabe, S. Nakamura, *Pharmaceutics* **2020**, *12*, 277.

[7] E. Everett, N. Mathioudakis, *Ann. N. Y. Acad. Sci.* **2018**, *1411*, 153.

[8] B. Li, S. Luan, J. Chen, Y. Zhou, T. Wang, Z. Li, Y. Fu, A. Zhai, C. Bi, *Mol. Ther. Nucleic Acids* **2019**, *19*, 814.

[9] P. Wu, H. Chen, R. Jin, T. Weng, J. Ho, C. You, L. Zhang, X. Wang, C. Han, *J. Transl. Med.* **2018**, *16*, 29.

[10] S. A. Eming, T. Krieg, J. M. Davidson, *Expert Opin. Biol. Ther.* **2004**, *4*, 1373.

[11] P. Y. Lee, Z. Li, L. Huang, *Pharm. Res.* **2003**, *20*, 1995.

[12] M. Kulkarni, A. O'Loughlin, R. Vazquez, K. Mashayekhi, P. Rooney, U. Greiser, E. O'Toole, T. O'Brien, M. M. Malagon, A. Pandit, *Biomaterials* **2014**, *35*, 2001.

[13] O. Veiseh, B. C. Tang, K. A. Whitehead, D. G. Anderson, R. Langer, *Nat. Rev. Drug Discovery* **2015**, *14*, 45.

[14] S. D. Bull, M. G. Davidson, J. M. H. Van Den Elsen, J. S. Fossey, A. T. A. Jenkins, Y. B. Jiang, Y. Kubo, F. Marken, K. Sakurai, J. Zhao, T. D. James, *Acc. Chem. Res.* **2013**, *46*, 312.

[15] W. Wu, S. Zhou, *Macromol. Biosci.* **2013**, *13*, 1464.

[16] A. E. Powell, M. A. Leon, *Cell Res.* **1970**, *62*, 315.

[17] M. G. Jeschke, D. Klein, *Gene Ther.* **2004**, *11*, 847.

[18] A. Jazwa, P. Kucharzewska, J. Leja, A. Zagorska, A. Sierpniowska, J. Stepniewski, M. Kozakowska, H. Taha, T. Ochiya, R. Derlacz, E. Vahakangas, S. Yla-Herttuala, A. Jozkowicz, J. Dulak, *Genet Vaccines Ther* **2010**, *8*, 6.

[19] S. E. Lynch, J. C. Nixon, R. B. Colvin, H. N. Antoniades, *Proc. Natl. Acad. Sci. USA* **1987**, *84*, 7696.

[20] J. Yu, J. Wang, Y. Zhang, G. Chen, W. Mao, Y. Ye, A. R. Kahkoska, J. B. Buse, R. Langer, Z. Gu, *Nat. Biomed. Eng.* **2020**, *4*, 499.

[21] L. R. Volpatti, M. A. Matranga, A. B. Cortinas, D. Delcassian, K. B. Daniel, R. Langer, D. G. Anderson, *ACS Nano* **2020**, *14*, 488.

[22] D. H. C. Chou, M. J. Webber, B. C. Tang, A. B. Lin, L. S. Thapa, D. Deng, J. V. Truong, A. B. Cortinas, R. Langer, D. G. Anderson, *Proc. Natl. Acad. Sci. USA* **2015**, *112*, 2401.

[23] D. Whelan, N. M. Caplice, A. J. P. Clover, *J Control Release* **2014**, *196*, 1.

[24] C. T. Drinnan, G. Zhang, M. A. Alexander, A. S. Pulido, L. J. Suggs, *J Control Release* **2010**, *147*, 180.

[25] M. Ehrbar, V. G. Djonov, C. Schnell, S. A. Tschanz, G. Martiny-Baron, U. Schenk, J. Wood, P. H. Burri, J. A. Hubbell, A. H. Zisch, *Circ. Res.* **2004**, *94*, 1124.

[26] D. J. Geer, D. D. Swartz, S. T. Andreadis, *Am. J. Pathol.* **2005**, *167*, 1575.

[27] W. Zhou, M. Zhao, Y. Zhao, Y. Mou, *J. Mater. Sci. Mater. Med.* **2011**, *22*, 1221.

[28] W. Vanscheidt, A. Ukat, V. Horak, H. Brüning, J. Hunyadi, R. Pavlicek, M. Emter, A. Hartmann, J. Bende, T. Zwingers, T. Ermuth, R. Eberhardt, *Wound Repair Regen* **2007**, *15*, 308.

[29] V. Falanga, S. Iwamoto, M. Chartier, T. Yufit, J. Butmarc, N. Kouttab, D. Shrayer, P. Carson, *Tissue Eng.* **2007**, *13*, 1299.

[30] B. C. Dash, S. Mahor, O. Carroll, A. Mathew, W. Wang, K. A. Woodhouse, A. Pandit, *J. Control Release* **2011**, *152*, 382.

[31] N. Laurens, P. Koolwijk, M. P. de Maat, *J. Thromb. Haemost.* **2006**, *4*, 932.

[32] A. Breen, T. O'Brien, A. Pandit, *Tissue Eng. Part B Rev.* **2009**, *15*, 201.

[33] M. Reth, *Nat. Immunol.* **2002**, *3*, 1129.

[34] H. A. Woo, S. H. Yim, D. H. Shin, D. Kang, D. Y. Yu, S. G. Rhee, *Cell* **2010**, *140*, 517.

[35] G. Zhu, Q. Wang, S. Lu, Y. Niu, *Med Princ Pract* **2017**, *26*, 301.

[36] J. V. Cordeiro, A. Jacinto, *Nat. Rev. Mol. Cell Biol.* **2013**, *14*, 249.

[37] C. Appenzeller-Herzog, G. Bánhegyi, I. Bogeski, K. J. A. Davies, A. Delaunay-Moisan, H. J. Forman, A. Görlach, T. Kietzmann, F. Laurindo, E. Margittai, A. J. Meyer, J. Riemer, M. Rützler, T. Simmen, R. Sitia, M. B. Toledano, I. P. Touw, *Biol. Med.* **2016**, *94*, 157.

[38] S. Vukelic, Q. Xu, B. Seidel-Rogol, E. A. Faidley, A. E. Dikalova, L. L. Hilenski, U. Jorde, L. B. Poole, B. Lassègue, G. Zhang, K. K. Griendling, *Arterioscler Thromb Vasc Biol* **2018**, *38*, 2423.

[39] M. M. Shi, I. W. Chong, J. J. Godleski, J. D. Paulauskis, *Immunology* **1999**, *97*, 309.

[40] M. M. Shi, J. J. Godleski, J. D. Paulauskis, *J. Biol. Chem.* **1996**, *271*, 5878.

[41] M. Jaramillo, M. Olivier, *J. Immunol.* **2002**, *169*, 7026.

[42] A. E. Loo, R. Ho, B. Halliwell, *Biol. Med.* **2011**, *51*, 884.

[43] A. E. K. Loo, Y. T. Wong, R. Ho, M. Wasser, T. Du, W. T. Ng, B. Halliwell, *PLoS One* **2012**, *7*, e49215.

[44] M. Cho, T. K. Hunt, M. Z. Hussain, *Am. J. Physiol. Hear. Circ. Physiol.* **2001**, *280*, H2357.

[45] M. Brauchle, J. O. Funk, P. Kind, S. Werner, *J. Biol. Chem.* **1996**, *271*, 21793.

[46] J. Ruef, Z. Y. Hu, L. Y. Yin, Y. Wu, S. R. Hanson, A. B. Kelly, L. A. Harker, G. N. Rao, M. S. Runge, C. Patterson, *Circ. Res.* **1997**, *81*, 24.

[47] S. Rieger, A. Sagasti, *PLoS Biol.* **2011**, *9*, e1000621.

[48] J. I. Ito, Y. Nagayasu, M. Hoshikawa, K. H. Kato, Y. Miura, K. Asai, H. Hayashi, S. Yokoyama, M. Michikawa, *Brain Res.* **2013**, *1522*, 12.

2300161 (18 of 18)